Amazon Plume Salinity Response to Ocean Teleconnections

Pedro Tyaquiçã, Dóris Veleda, Nathalie Lefèvre, Moacyr Araujo, Carlos Noriega, Guy Caniaux, Jacques Servain, Thiago Silva

▶ **To cite this version:**

Pedro Tyaquiçã, Dóris Veleda, Nathalie Lefèvre, Moacyr Araujo, Carlos Noriega, et al.. Amazon Plume Salinity Response to Ocean Teleconnections. Frontiers in Marine Science, 2017, 4, pp.250. 10.3389/fmars.2017.00250 . hal-01686382

HAL Id: hal-01686382
https://hal.science/hal-01686382

Submitted on 6 Jan 2021

HAL is a multi-disciplinary open access archive for the deposit and dissemination of scientific research documents, whether they are published or not. The documents may come from teaching and research institutions in France or abroad, or from public or private research centers.

L'archive ouverte pluridisciplinaire **HAL**, est destinée au dépôt et à la diffusion de documents scientifiques de niveau recherche, publiés ou non, émanant des établissements d'enseignement et de recherche français ou étrangers, des laboratoires publics ou privés.

Distributed under a Creative Commons Attribution - NonCommercial 4.0 International License

frontiers in Marine Science

ORIGINAL RESEARCH
published: 03 August 2017
doi: 10.3389/fmars.2017.00250

Amazon Plume Salinity Response to Ocean Teleconnections

Pedro Tyaquiçã[1,2], Doris Veleda[1,2], Nathalie Lefèvre[3], Moacyr Araujo[1,2], Carlos Noriega[1,2], Guy Caniaux[4], Jacques Servain[3,5] and Thiago Silva[1,6]*

[1] Department of Oceanography, DOCEAN, Federal University of Pernambuco, Recife, Brazil, [2] Brazilian Research Network on Global Climate Change (Rede CLIMA), São Paulo, Brazil, [3] IRD-LOCEAN—Institut de Recherche pour le Développement, Sorbonne Universités, Paris, France, [4] CNRM/UMR 3589, Météo-France and Centre de la Recherche Scientifique, Toulouse, France, [5] Fundação Cearense de Meteorologia e Recursos Hídricos, Fortaleza, Brazil, [6] Agência Pernambucana de Águas e Clima, Recife, Brazil

Pacific and Atlantic sea surface temperature (SST) variability strongly influences rainfall changes in the Amazon River basin, which impacts on the river discharge and consequently the sea surface salinity (SSS) in the Amazon plume. An Empirical Orthogonal Function (EOF) analysis was performed using 46 years of SST, rainfall, and SSS datasets, in order to establish the relationship between these variables. The first three modes of SST/rainfall explained 87.83% of the total covariance. Pacific and Atlantic SSTs led Amazon basin rainfall events by 4 months. The resultant SSS in the western tropical North Atlantic (WTNA) lagged behind basin rainfall by 3 months, with 75.04% of the total covariance corresponding to the first four EOF modes. The first EOF mode indicated a strong SSS pattern along the coast that was connected to negative rainfall anomalies covering the Amazon basin, linked to El Niño events. A second pattern also presented positive SSS anomalies, when the rainfall was predominantly over the northwestern part of the Amazon basin, with low rainfall around the Amazon River mouth. The pattern with negative SSS anomalies in the WTNA was associated with the fourth mode, when positive rainfall anomalies were concentrated in the northwest part of South America. The spatial rainfall structure of this fourth mode was associated with the spatial rainfall distribution found in the third EOF mode of SST vs. rainfall, which was a response to La Niña Modoki events. A statistical analysis for the 46 year period and monthly anomaly composites for 2008 and 2009 indicated that La Niña Modoki events can be used for the prediction of low SSS patterns in the WNTA.

Keywords: El Niño, sea surface temperature, rainfall, sea surface salinity, Amazon River plume

OPEN ACCESS

Edited by:
Ajit Subramaniam, Lamont Doherty Earth Observatory, Columbia University, United States

Reviewed by:
Gregory Foltz, Atlantic Oceanographic and Meteorological Laboratory (NOAA), United States
Gael Alory, UMR5566 Laboratoire D'études en Géophysique et Océanographie Spatiales (LEGOS), France

****Correspondence:***
Pedro Tyaquiçã
pedro.tssantos@ufpe.br

Specialty section:
This article was submitted to Aquatic Microbiology, a section of the journal Frontiers in Marine Science

Received: *30 April 2017*
Accepted: *21 July 2017*
Published: *03 August 2017*

Citation:
Tyaquiçã P, Veleda D, Lefèvre N, Araujo M, Noriega C, Caniaux G, Servain J and Silva T (2017) Amazon Plume Salinity Response to Ocean Teleconnections. Front. Mar. Sci. 4:250. doi: 10.3389/fmars.2017.00250

INTRODUCTION

Ocean salinity is an indicator of changes in the global hydrological cycle and large-scale climate variability (Du et al., 2015). The spatial distribution of salt in the ocean and its seasonal and interannual variability are important for understanding Earth's climate. Ocean salinity has an important role in the thermohaline circulation and the distribution of mass and heat. The spatial distribution of sea surface salinity (SSS) in the global ocean also reflects the pattern of air-sea freshwater fluxes, evaporation and precipitation, heat, momentum, solubility, and the biological pump (Geider et al., 2001; Yu et al., 2007; Schmitt, 2008; Du et al., 2015). Changes

in salinity patterns indicate where terrestrial and marine systems mix, which is where nutrients are distributed, and in turn impacts on the production of coastal and oceanic ecosystems (Smith and Demaster, 1996; Araujo et al., 2014). The Amazon River is by far the largest single source of terrestrial freshwater to the ocean, contributing ∼20–30% of the total river discharge to the Atlantic (Wisser et al., 2010; Salisbury et al., 2011; Korosov et al., 2015). SSS in the western tropical North Atlantic (WTNA) is strongly influenced by the Amazon River discharge, advection by surface currents, and rainfall (Grodsky et al., 2015; Ibánhez et al., 2017). The low salinity Amazon plume creates a near-surface barrier layer that inhibits mixing, increases the sea surface temperature (SST), and enhances salinity stratification; thus, preventing vertical mixing between the upper warm mixed layer and the cold deep ocean (Ferry and Reverdin, 2004; Balaguru et al., 2012; Grodsky et al., 2012; Coles et al., 2013).

The latitudinal displacement of the Intertropical Convergence Zone (ITCZ) in association with high precipitation modifies the surface conditions, following the input of freshwater inputs from large rivers. Ibánhez et al. (2017) compared the monthly precipitation rate with monthly SSS in five regions of the tropical Atlantic. They found significant linear relationships of precipitation with SSS across the western Atlantic basin. The extension of the Amazon River plume is significant, with a range of 0.25–1.60 $\times$ 10^6 km^2 after removing the influence of rainfall. The intense rainfall associated with the ITCZ has led to a significant overestimation of the spatial extension of the Amazon River plume in previous studies (Körtzinger, 2003; Lefèvre et al., 2010).

The Amazon plume is transported by the North Brazilian Current (NBC) near the equator and is carried northwestward along the Brazilian Shelf toward the Caribbean Sea (Muller-Krager et al., 1988; Salisbury et al., 2011). The eastward propagation of Amazon waters is observed when the retroflection of the NBC takes place. The seasonal variations in these currents occurs in response to the annual migration of the ITCZ, which leads to the northward transport of Amazon water in the austral winter, and the eastward transport of Amazon water into the North Equatorial Counter Current (NECC) in the austral spring through fall (Muller-Krager et al., 1988; Lentz, 1995; Coles et al., 2013; Foltz et al., 2015). The fresh and cold waters of the Amazon River are then transported hundreds to thousands of kilometers away from the coast, and the nutrients delivered by the river plume contribute to the enhancement of primary production; thus, contributing to carbon sequestration (Subramanian et al., 2008).

The Amazon River discharge is also affected by remote climatic signals via Amazon basin rainfall variability that is under different influences from the Pacific and Atlantic tropical oceans. The influence of the El Niño Southern Oscillation (ENSO) on seasonal precipitation anomalies over South America has been extensively studied (Marengo, 1992; Uvo et al., 1998; Grimm et al., 2000; Paegle and Mo, 2002; Ronchail et al., 2002; Grimm, 2003, 2004; Misra, 2008a). ENSO influences the large-scale east–west and meridional circulations in the global tropics that have consequences over tropical South America (Grimm, 2003, 2004; Misra, 2008b).

The rainfall over the Amazon basin and northeast Brazil has a distinct interannual variability, in part due to the climate signals in the tropical Pacific from the ENSO and to the meridional SST gradient in the tropical Atlantic (Marengo et al., 2013). This modifies the spatial and temporal Amazon rainfall variability, consequently affecting the Amazon plume. Recent studies have shown that the canonical ENSO has become less frequent, while a different kind of ENSO in the central Pacific, called the Modoki ENSO, is occurring more frequently and has become more common during the late twentieth century (Ashok et al., 2007; Ashok and Yamagata, 2009; Kao and Yu, 2009; Yeh et al., 2009; Yu et al., 2010; Li et al., 2011; McPhaden et al., 2011). The traditional ENSO is characterized by strong anomalous warming in the eastern equatorial Pacific. In contrast, the Modoki ENSO phenomenon is characterized by an anomalous warm SST in the central equatorial Pacific, flanked by anomalously cool regions in both the west and east. The teleconnections associated with these distinct warming and cooling patterns are very different from those of the conventional ENSO (Yeh et al., 2009).

Weng et al. (2007) performed a correlation analysis between Global Precipitation Climatology Centre (GPCC) rainfall rate anomalies and the El Niño Modoki Index (EMI) and Niño 3. They identified positive and negative rainfall anomalies over northwest South America related to Niño 3. However, during Modoki El Niño events, they found negative rainfall anomalies over the east Pacific and positive rainfall anomalies in the western part of the Amazon basin. Because of the conclusions of this and other studies, the Modoki ENSO is considered to be a new driver of global climate change (Xie et al., 2014) and is being linked to global warming (Yeh et al., 2009). Based on the detection of the principal Empirical Orthogonal Function (EOF) analysis modes, this study identified the coupled modes of variability between SSTs and rainfall over the Amazon basin, and between Amazon rainfall and SSS over the Amazon plume in the WTNA to better understand the climate impacts on biogeochemical cycles in the WTNA.

METHODS

Datasets

Datasets containing 46 year (January 1970 to December 2015) records of SST, rainfall, and SSS were used to conduct the analysis. SST monthly data were obtained from the Ocean ReAnalysis System 4 (ORAS4: http://icdc.cen.uni-hamburg.de/), with 1° $\times$ 1° grid resolution. ORAS4 was evaluated by comparison with observed ocean currents, derived transport, sea-level gauges, and bottom pressure (Balmaseda et al., 2013). The monthly rainfall data were obtained from the GPCC, full data reanalysis version 7 (GPCC v7: http://www.esrl.noaa.gov/psd/). The GPCC v7 provides global land-surface rainfall in a regular grid, with a resolution of 1° $\times$ 1°. This dataset is based on 75,000 gauges located worldwide and enables the analysis of climate variability and historical trends (Schneider et al., 2014, 2015). The Global Precipitation Climatology Project (GPCP), version 2.3, with 2.5° resolution was also used to determine anomalies of land and oceanic rainfall. In addition to SST, SSS was also obtained from the ORAS4 database, with the same spatial and temporal resolution.

We also used data for 46 years of monthly Amazon discharge values recorded at the Óbidos Gauging Station, which was available from the Environmental Research Observatory–Geodynamical, hydrological, and biogeochemical control of erosion/alteration and material transport in the Amazon basin (ORE–HYBAM: http://www.ore-hybam.org). The values recorded at the Óbidos Gauging Station, about 600 km west of the river mouth, were used to estimate the interannual variability of the Amazon River discharge.

In this study, we used data for 46 years of monthly zonal, meridional, and vertical components of winds from ERA-Interim reanalysis, produced by the European Centre for Medium-Range Weather Forecasts (ECMWF), and available at http://www.ecmwf.int/.

Statistical Analysis

The influence of the Pacific and Atlantic SST on rainfall over South America and the rainfall distribution on SSS in the Amazon River plume on an interannual timescale was analyzed by applying a coupled EOF analysis. The EOF was constructed by a Singular Value Decomposition (SVD) analysis (Bretherton et al., 1992; Wallace et al., 1992) of the cross-covariance matrix between SST (140°–20°E, 20°S–20°N) and rainfall (20°S–20°N and 80°W–20°E) for the dataset period. SVD was conducted by analyzing the covariance matrix between Pacific and Atlantic SSTs and precipitation anomalies over South America, and was conducted after the monthly climatologies were removed from the SST, rainfall, and SSS datasets.

From this analysis, we computed the loadings and scores for both modes, SST vs. rainfall and rainfall vs. SSS. These loadings were computed from the left and right eigenvectors and represented the spatial patterns of the corresponding mode. The scores of the SVD modes were computed by projecting the data on to the loadings of the corresponding field. The squared covariance fraction (SCF) expresses the percentage explained by the modes. One of the benefits of SVD is that the order of the calculated modes is based on the strength of their co-variability, as the first mode is the strongest and the last mode is the weakest. To identify the connection between rainfall EOF patterns, a linear regression analysis was performed between the rainfall vs. SSS principal components (PCs) and SST vs. rainfall PCs.

To improve the analysis of rainfall behavior over the Amazon basin, the PCs from each EOF were correlated with Pacific and Atlantic climatic indices (**Table 1**). The statistical significance of the cross-correlations between climate indices and the PCs was determined from a two-sample *t*-test at 95% confidence levels. The climatic indices were obtained from the Earth System Research Laboratory/National Oceanic and Atmospheric Administration (ESRL/NOAA), and are available at https://www.esrl.noaa.gov/.

TABLE 1 | ENSO and Atlantic indices and respective regions of SST anomalies.

Index	Covered area
Niño12	El Niño 1+2. Area-averaged SST anomaly over Extreme Eastern Pacific SST, from equator to 10°S, 90°–80°W
Niño3	El Niño 3. Area-averaged SST anomaly over Eastern Tropical Pacific SST, 5°N–5°S, 150° W–90°W
Niño34	El Niño 3.4. Area-averaged SST anomaly over East Central Pacific SST, 5°N–5°S, 170°–120°W
Niño4	El Niño 4. Area-averaged SST anomaly over Central Pacific SST, 5°N–5°S, 160°E–150°W
EMI	El Niño Modoki Index. Computed by combining SST anomalies averaged over each box-area, A−(B+C)/2. Where: A (165°E–140°W, 10°S–10°N), B (110°–70°W, 15°S–5°N) and, C (125°–145°E, 10°S–20°N)
NTA	North Tropical Atlantic SST Index. SST anomalies averaged over 60°W–20° W, 6°–18°N and 20°–10°W, 6°–10°N
TNA	Tropical Northern Atlantic Index. SST anomalies averaged over 57.5°–15°W and 5.5°–23.5°N
TSA	Tropical Southern Atlantic Index. SST anomalies averaged over Eq–20°S and 10°E–30°W
AMM	Atlantic Meridional Mode. Maximum Covariance Analysis (MCA) to sea surface temperature (SST) and the zonal and meridional components of the 10 m wind field over the time period 1950-2005, from the NCEP/NCAR Reanalysis. The spatial pattern cover 21°S–32°N, 74°W–15°E
CTA	Cold tongue anomaly, SST anomalies averaged over 10°W–15°E and 5°N–5°S

RESULTS AND DISCUSSION

Pacific and Atlantic SST vs. Amazon Basin Rainfall

The distinct patterns of SST anomalies in the Pacific and Atlantic oceans induced different rainfall responses over the watershed of the Amazon basin and this subsequently influenced the river discharge. The results of the EOFs performed between SST and rainfall reflected this behavior. The EOF analysis was performed with rainfall lagging SST by 1–4 months. SST acted as the predictor and precipitation acted as the response series. The results were limited to a 4 month-lagged cross-covariance matrix, with rainfall lagging SST, based on the best response relation. This EOF analysis of the lagged cross-covariance matrix between tropical Pacific and Atlantic SST and rainfall in the Amazon basin revealed three main modes. These modes together explained 87.83% of the total covariance between SST and rainfall, with 73.89, 7.91, and 6.03% of the signal explained by EOF1, EOF2, and EOF3 respectively. The PC1 SST signal was correlated with El Niño 3 (0.94, $p < 0.05$). In the canonical El Niño phase, SST anomalies over tropical and subtropical latitudes were warmer than normal. The spatial pattern of EOF1 (**Figure 1**) was characterized by a basin-scale warming from the eastern to central Pacific, which was negatively associated with rainfall in the northeast Amazon basin portion. Rainfall during a canonical El Niño event was increased in the west coast regions of South America, while La Niña events increased rainfall over central South America and the Amazon basin. The regions in the Amazon basin that received most rainfall corresponded to the western portion of the watershed near the Andean elevation. Below average rainfall covered the central and eastern areas of the basin, near the river mouth.

It is known from previous work that on interannual timescales the ENSO system has a large variance in the Pacific (Yeh and Kirtman, 2004; Di Lorenzo et al., 2015). Jiménez-Muñoz

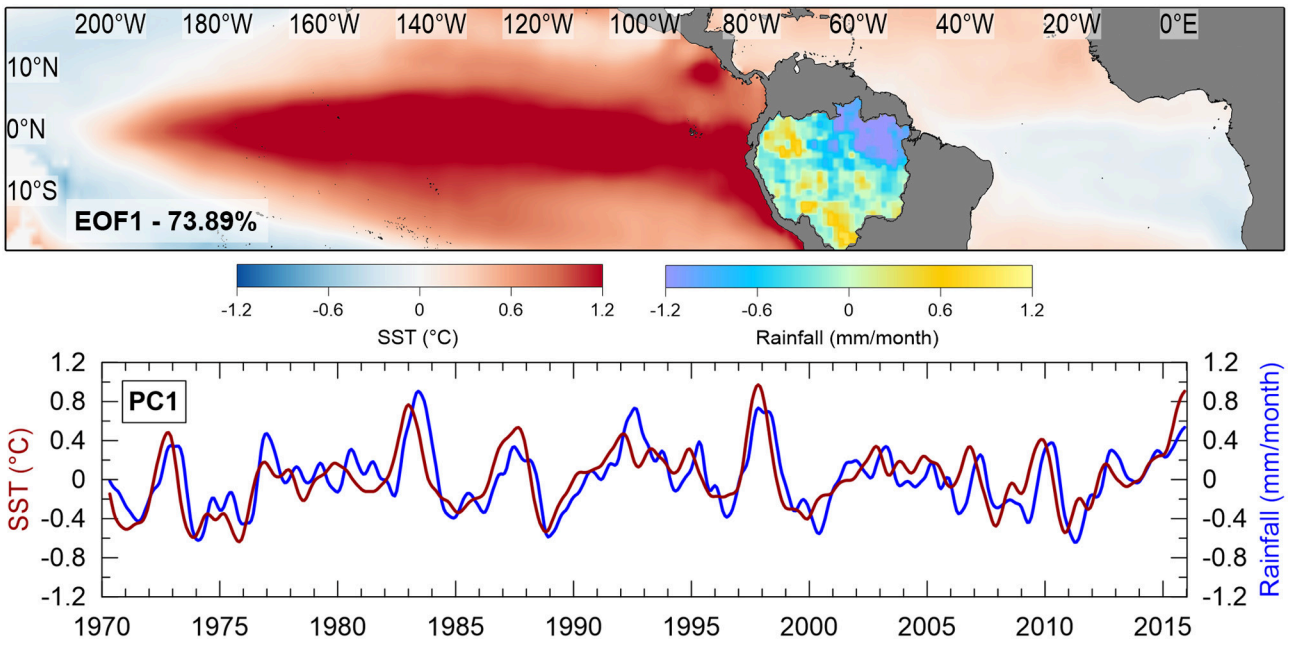

FIGURE 1 | First EOF mode of 4 month-lagged covariance matrix between SST and rainfall (normalized scale by 10^3), the Squared Covariance Fraction (SCF) in percentage, and the first Principal Component (PC1).

et al. (2016) have classified the 2015/2016 El Niño event as an unprecedented warming, with extreme drought in Amazonia compared to the earlier strong El Niño events of 1982/83 and 1997/98. They found that both eastern and central Pacific SST anomalies in December 2015 contributed to this ENSO, with a strong decay from January to June 2016, which was characterized by a stronger contribution from the central Pacific.

As shown in **Figure 1**, the Pacific SST anomalies in the Pacific Ocean were most often present near the South American coast, dispersing westward through the ocean, with a pattern similar to El Niño 3. Following this SST pattern, rainfall was more concentrated in the westward and southwestward portion of the Amazon basin. El Niño 3 events are associated with periodic severe droughts in Amazonia due to convective inhibition and rainfall reduction in the northern, eastern, and western parts of Amazonia (Marengo and Espinoza, 2015). Some of this reduction in rainfall in Amazonia is associated with canonical El Niño events, with a contribution from the Atlantic. This increase in SST would weaken the northeast trade winds, reducing the moisture transport from the tropical Atlantic into the Amazon region.

PC2 (**Figure 2**), which corresponded to 7.91% of the variance, was negatively correlated with the cold tongue anomaly (CTA) (-0.74, $p < 0.05$). The EOF2 pattern was characterized by sparse positive rainfall anomalies mainly in the central part of the Amazon basin (**Figure 2**). The sparse rainfall distribution was weakly correlated with Pacific climatic indices, but there were stronger negative correlations with the equatorial and North Atlantic (**Table 2**). Marengo (1992) and Marengo et al. (2008) reported that cold SST events in the North Atlantic were associated with stronger northeast trade winds and an increase in moisture transport from the North Atlantic into the Amazon.

The spatial pattern of EOF3 (**Figure 3**) corresponded to 6% of the covariance and exhibited a zonal structure in the cooling of SSTs in the central Pacific and a warming in the eastern Pacific. PC3 (**Figure 3**) was negatively correlated with the EMI (-0.83, $p < 0.05$) (**Table 2**). The PC (**Figure 3**) associated with this mode corresponded to the negative phase of the Modoki ENSO (La Niña Modoki). The negative correlation presented in the EOF3 indicated that the positive rainfall anomalies over northwest South America responded to La Niña Modoki events. La Niña Modoki events have received less attention than prominent canonical La Niña events observed in the central Pacific due to the difficulty in identifying distinct types of cold events (Shinoda et al., 2011; Kulkarni and Siingh, 2016). Despite the PC correlation with the negative phase of Modoki El Niño and canonical La Niña events being similar, the spatial structure of SSTs (**Figure 3**) was characterized by a cold area in the central Pacific and a warmer area in the eastern Pacific, which is a characteristic of La Niña Modoki events (Ashok et al., 2007). The corresponding EOF3 spatial pattern of rainfall over the continent is shown in **Figure 3**, and indicated positive rainfall anomalies in the northwestern part of the Amazon basin. This is the area that makes the largest contribution to the Amazon River discharge and is formed mainly by the junction of the Negro River, coming from the northwest, and the Solimões River (Beluco and Souza, 2014).

A similar spatial pattern was also reported by Ashok et al. (2007), although they performed a single EOF of SSTs over the Pacific, from 1979 to 2004. They identified the first mode as a canonical El Niño event (45%), with the second mode

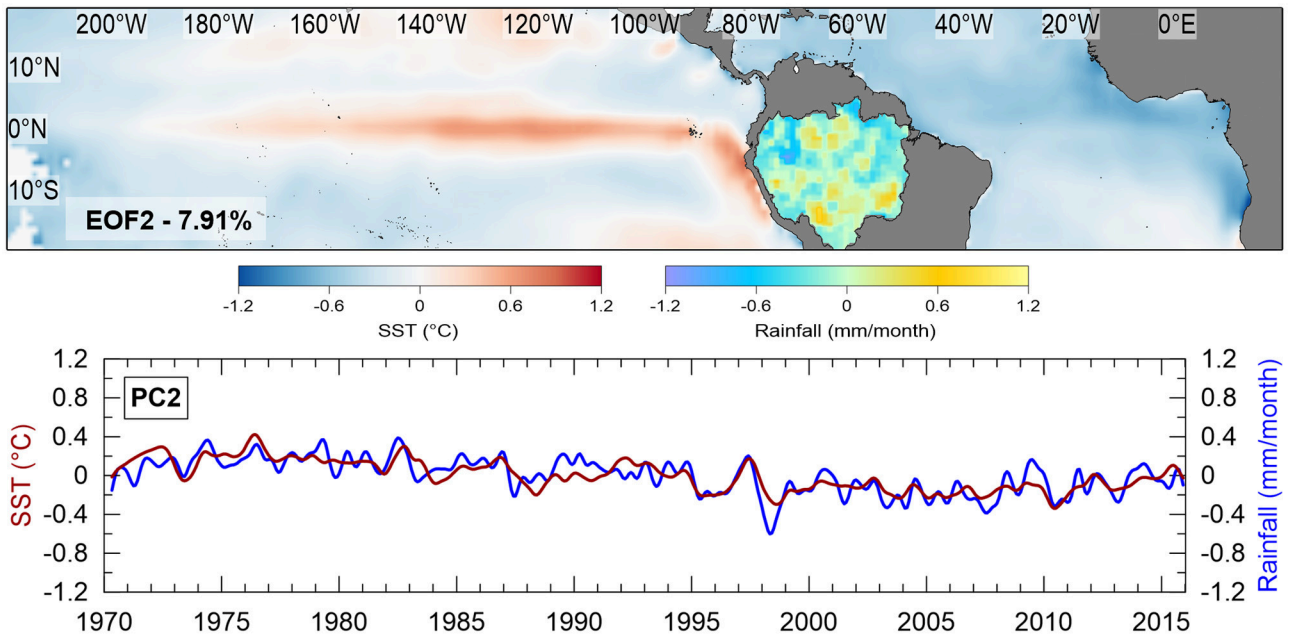

FIGURE 2 | Second EOF of 4 month-lagged covariance matrix between SST and rainfall (normalized scale by 10^3), the Squared Covariance Fraction (SCF) in percentage, and the second Principal Component (PC2).

TABLE 2 | Forty-six years Cross-correlation between PCs of 4 month-lagged EOF SST × Rainfall with Pacific and Atlantic Indices.

	Niño12 *dof = 95*	Niño3 *dof = 98*	Niño34 *dof = 92*	Niño4 *dof = 71*	TNA *dof = 17*	TSA *dof = 68*	AMM *dof = 47*	CTA *dof = 16*	EMI *dof = 63*
PC1 SST	**0.80***	**0.94***	**0.94***	**0.85***	**0.25***	−0.01	−0.03	0.03	**0.43***
PC2 SST	**0.15***	**0.12***	**0.12***	−0.06	**−0.62***	**−0.58***	**−0.46***	**−0.75***	0.06
PC3 SST	**0.32***	−0.04	**−0.28***	**−0.56***	**−0.09***	−0.04	−0.03	**−0.13***	**−0.83***

The cross-correlations in bold are significant with 95% confidence level. The effective number of degrees of freedom (dof) was calculated by the autocorrelation scale.
**α = 0.05; dof, degrees of freedom; cc, cross-correlation.*

corresponding to the Modoki signal explaining 12% of the SST variability, the third mode explaining 7%, and the fourth mode explaining 4.5%. Using SST composites, the authors identified two seasonal Modoki events. The first one, which occurred in the austral winter (June–September), was warmer in the central Pacific and extended northeastward in the North Atlantic and southeastward in the South Atlantic. The other mode was confined to the equatorial Pacific from December to February.

Amazon Basin Rainfall vs. WTNA SSS

The EOF spatial patterns of South American rainfall vs. SSS over the western tropical WTNA covered the area from 20°S to 20°N and 80°W to 20°E. The best response (i.e., stronger correlations) of SSS to the South American rainfall variability occurred with a 3-month lag. Results were limited to the coupled EOF with 3 month-lagged SSS. The first four modes retained 70.49% of the total covariance between SSTs and rainfall.

The first and third spatial modes of rainfall over South America showed a similar pattern to those found for the rainfall patterns of the coupled EOF of SST vs. rainfall.

The first mode explained 43.46% of the covariance (**Figure 4**). The rainfall pattern over the continent corresponded to the spatial pattern found in the first mode between SST and rainfall with a correlation of 0.96 ($p < 0.05$) (EOF1, **Figure 1**), which was associated with canonical El Niño events (**Table 2**). The negative rainfall over the Amazon basin was mostly attributed to canonical El Niño events, with strong droughts experienced in the Amazon basin in 1983, 1997, 2005, and 2010 (Marengo et al., 2013). As expected, this rainfall pattern was associated with high SSS along the coast, indicating that negative rainfall anomalies contributed to a low river discharge and consequently high SSS in the WTNA. This high SSS was present along the coast propagating northwestward. At about 50–55°W part of this signal was characterized by an eastward retroflection, with a zonal axis and maximum SSS centered at about 6°–8°N (**Figure 4**). The eastward NBC retroflection entered the western part of the NECC, transporting salty water that was still detectable until it reached 30°W. Similar structures were also detected by Grodsky et al. (2014a,b), during periods when the Amazon River discharge was low, and salty surface water from the southwestern equatorial

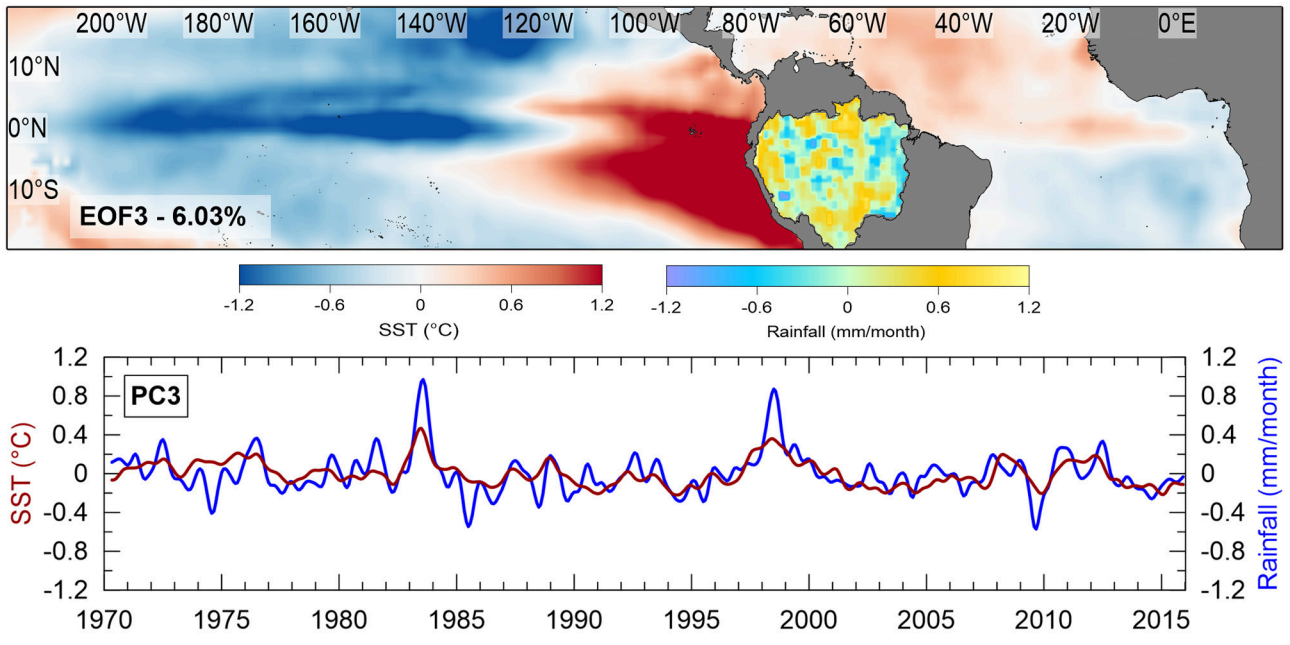

FIGURE 3 | Third EOF of 4 month-lagged covariance matrix between SST and rainfall (normalized scale by 10^3), the Squared Covariance Fraction (SCF) in percentage, and the third Principal Component (PC3).

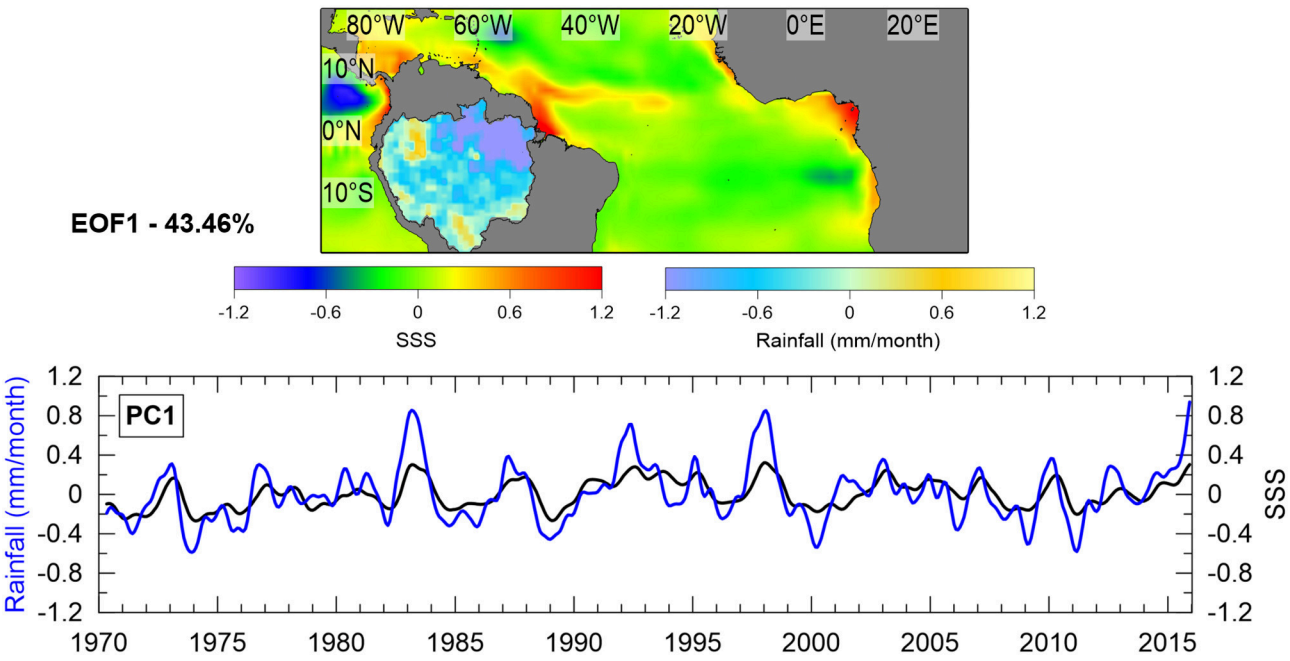

FIGURE 4 | First EOF of 3 month-lagged covariance matrix between rainfall (normalized scale by 10^3) and SSS (normalized scale by 10), the Squared Covariance Fraction (SCF) in percentage, and the first Principal Component (PC1).

Atlantic was transported by the NBC. North of 10°N and west of 50°W there was a core of low SSS, while to the east the low SSS propagated along 10°N. Some studies have described low salinity cores near Caribbean islands, trapped within NBC rings (Johns et al., 1998; Kelly et al., 2000; Hellweger and Gordon, 2002), with typical diameters up to 400 km and a life time of about 100 days.

EOF2 (**Figure 5**) explained about 14% of the covariance. The spatial distribution of rainfall over the continent indicated sparse positive rainfall anomalies over the western part of the

Amazon basin decreasing to the east, while negative rainfall anomalies were present near the Amazon River mouth. This pattern was associated with a high SSS that was confined to areas near the coast and transported northwestward, with part of this turning right. This eastward pathway that transported the higher salinities followed the NECC meanders, and enclosed a low salinity core with negative SSS anomalies.

EOF3 (**Figure 6**) corresponded to 7.54% of the covariance and presented positive rainfall anomalies in the western part of the Amazon basin and negative rainfall anomalies mainly in the

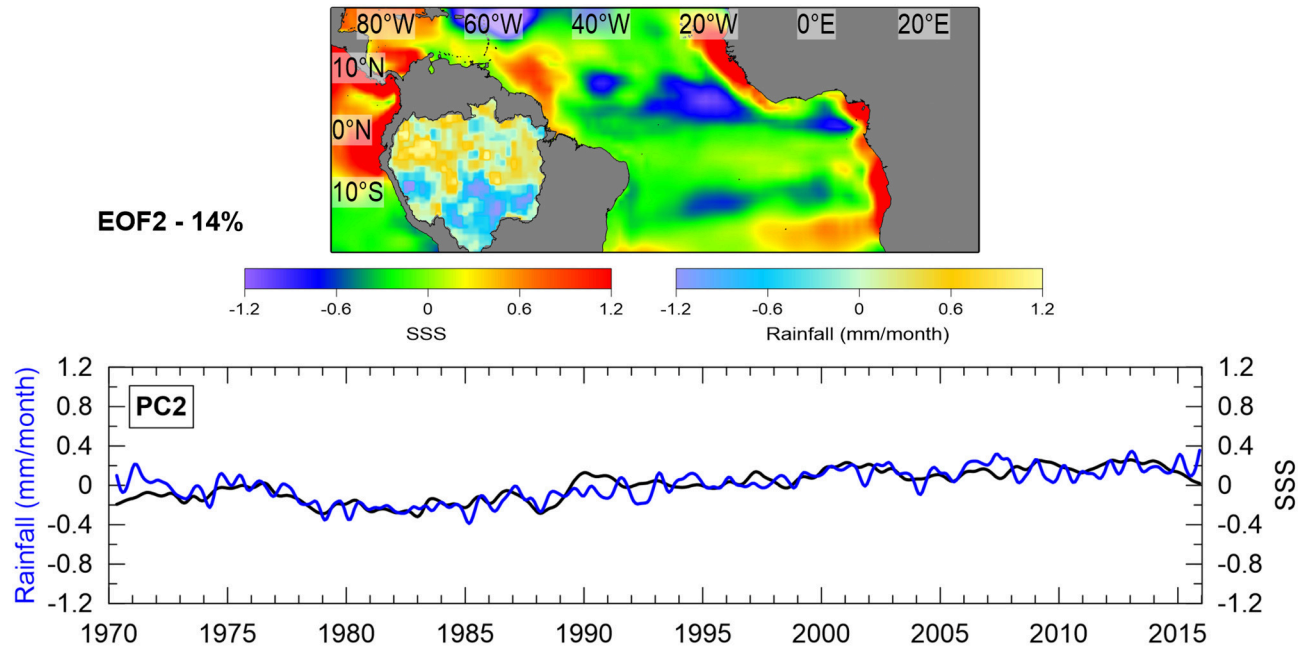

FIGURE 5 | Second EOF of 3 month-lagged covariance matrix between rainfall (normalized scale by 10^3) and SSS (normalized scale by 10), the Squared Covariance Fraction (SCF) in percentage, and the second Principal Component (PC2).

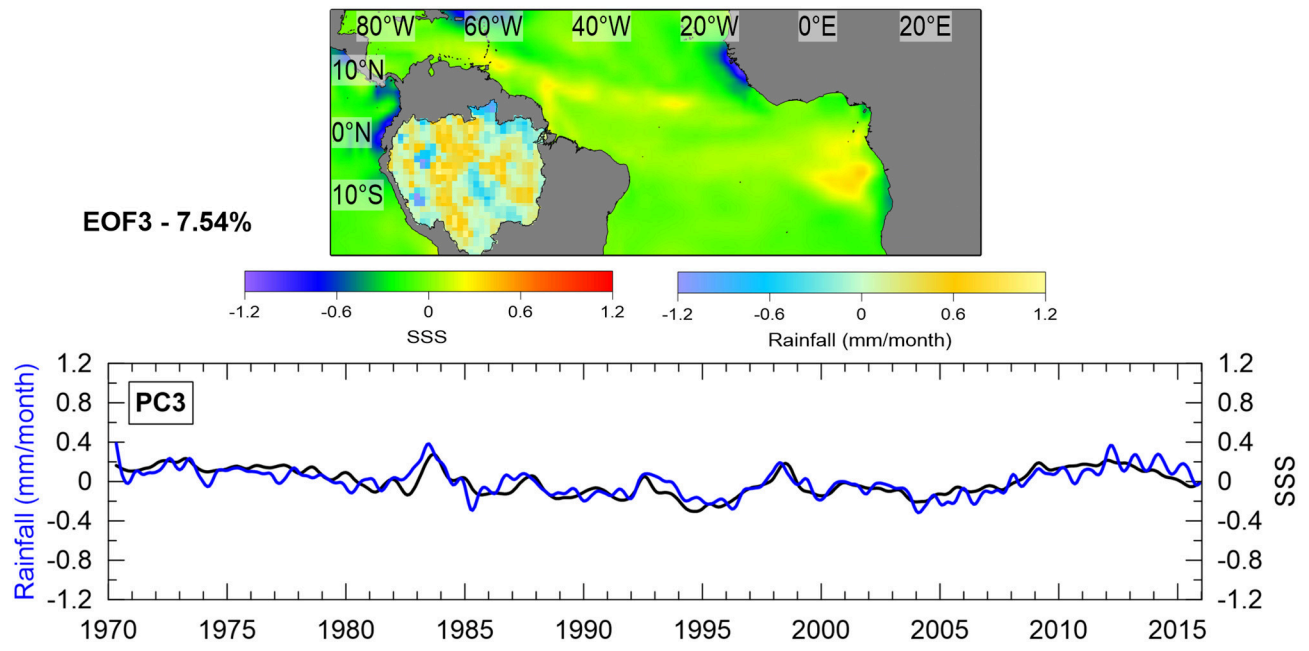

FIGURE 6 | Third EOF of 3 month-lagged covariance matrix between rainfall (normalized scale by 10^3) and SSS (normalized scale by 10), the Squared Covariance Fraction (SCF) in percentage, and the third Principal Component (PC3).

northeastern area along the coast. This pattern is associated with a northward axis (50°W) of positive SSS anomalies. This SSS signal was similar to the first mode; however, it was weaker and also had an eastward pathway between 6 and 8°N, following the NECC.

Figure 7 shows EOF4, which was between rainfall and SSS and explained 5.51% of the covariance. This rainfall pattern was similar to the rainfall structure of the third mode of the coupled EOF between SST and rainfall, which explained 6% of the covariance (EOF3, **Figure 3**), and was associated with cold equatorial waters in the central Pacific and warm waters in the eastern part of the Pacific. It was significantly negatively correlated with the negative phase of Modoki El Niño events (−0.83, **Table 2**). EOF4 presented positive rainfall anomalies mainly along the Orinoco and Negro basins in the northern area of northeast Brazil. This pattern showed a low-salinity plume emanating from the Amazon mouth in the WTNA, with a retroflection centered at 50°W and an eastward propagation along 6–8°N. The most striking pattern was the way the Amazon plume responded to the NBC and NECC.

In our EOF analysis, similar spatial rainfall patterns were found between the EOF1 SST vs. rainfall and EOF1 rainfall vs. SSS, and between EOF3 SST vs. rainfall and EOF4 rainfall vs. SSS. The relationships between these spatial structures were investigated through a linear regression between the respective PCs. The scatterplot (**Figure 8**) revealed a strong linear

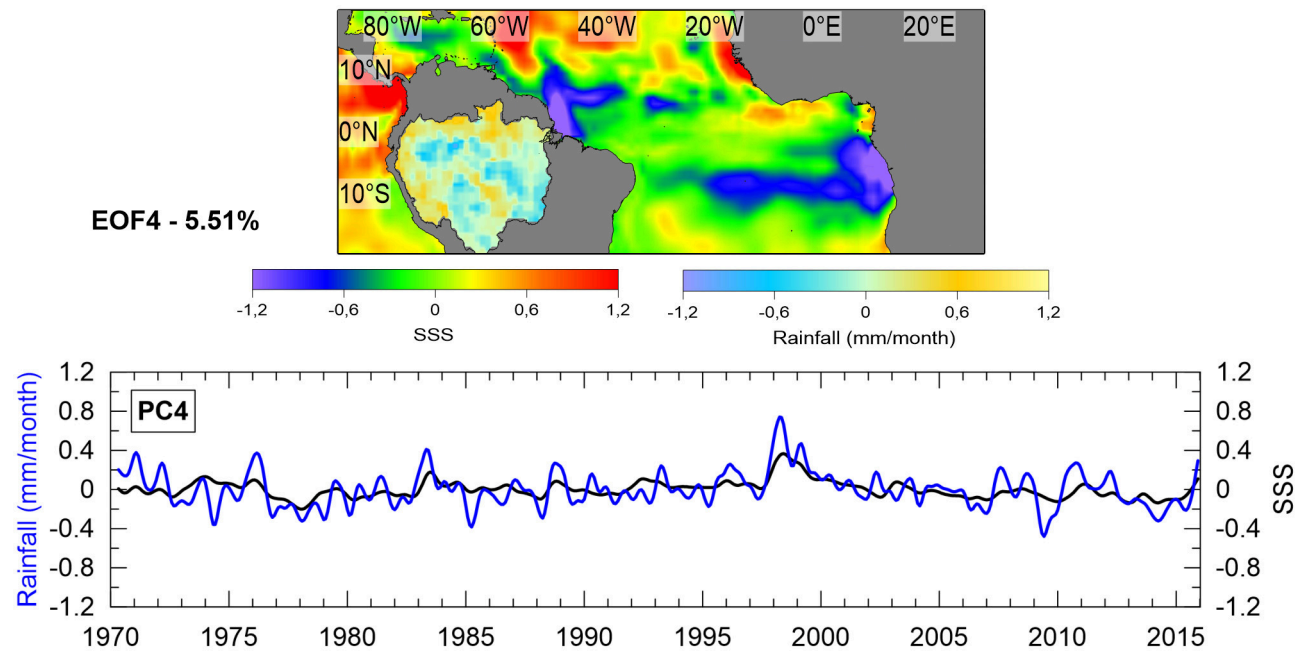

FIGURE 7 | Fourth EOF of 3 month-lagged covariance matrix between rainfall (normalized scale by 10^3) and SSS (normalized scale by 10), the Squared Covariance Fraction (SCF) in percentage, and the fourth Principal Component (PC4).

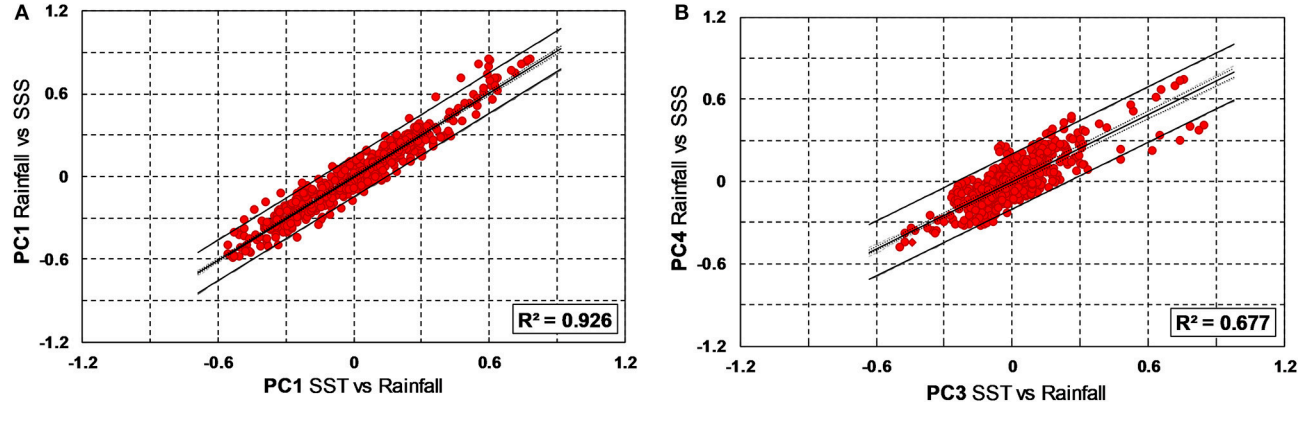

FIGURE 8 | Linear regression between **(A)** the first PCs of EOF rainfall vs. SSS by EOF SST vs. rainfall and, **(B)** the fourth PC of EOF rainfall vs. SSS by the third PC of SST vs. rainfall, both at 95% confidence level.

relationship between the first PCs of rainfall in both cases, with an R^2 of 0.92 and the fourth PC of rainfall associated with SSS corresponded to the third PC of rainfall associated with the SST, with an R^2 of 0.67, both at a 95% confidence level. These results confirm that the rainfall patterns associated with El Niño 3.4 and the EMI were the same as those present in the analysis between rainfall and SSS. The structure found in EOF4 differed from the other EOF modes. The fourth mode showed strong negative SSS anomalies that were associated with the high rainfall in the northwestern Amazon basin; however, the origin of the low salinity remained unclear, because part of this low salinity could also be a contribution from the ITCZ. Our analyses considered rainfall only over the continent, but the SSS signal had an influence from both the continent and rainfall over the ocean.

For example, in 2009 and 2012, the most serious floods of the last 40 years were recorded at the Manaus and Óbidos stations, due to the rising levels of the Solimões and Negro rivers, the two main branches of the Amazon River (Marengo et al., 2013). It is important to note that a strong and continuous La Niña Modoki occurred throughout 2008 (Shinoda et al., 2011). However, in 2009 there was also a very strong southern meridional event that was apparently not related to El Niño, which caused a very high anomalous change in the southern ITCZ and severe flooding in northeast Brazil. This southern mode was reported by Foltz et al. (2012). They argue that the anomalous cooling of SSTs in the equatorial North Atlantic triggered a strong southern-mode Atlantic event in April–May, with smaller SSTs in the equatorial North Atlantic and warmer SSTs in the equatorial South Atlantic. This event was characterized by abnormal north winds, causing an anomalous southward shift of the ITCZ and resulting in severe flooding in northeast Brazil.

In this study, we focused on 2009, because of the possible Atlantic oceanic influence in this year, whereas in 2012 there were no strong Atlantic SST anomalies. To better understand the role of the anomalous meridional shift in April–May 2009 and the previous La Niña Modoki event in 2008, in rainfall over the continent, we performed 3-month composites of SSTs, rainfall, and surface wind anomalies, for the period of December of 2007 to November 2009 (**Figure 9**).

The evolution of the composites indicated an anomalous SST cooling in the Pacific at the beginning of 2008, with positive rainfall anomalies over the southeastern basin and northeast Brazil. During this period, the eastern north Atlantic was characterized by anomalously warmer SSTs and the western north Atlantic was colder than normal.

From March to May of 2008, cooler waters were present in the central Pacific, which was associated with the warm SSTs in the Eastern Pacific. This indicated a well-defined La Niña Modoki, and was reported by Shinoda et al. (2011). Higher than normal rainfall was concentrated in the northwestern part of the Amazon basin, while SST positive anomalies intensified in the eastern North Atlantic and the western North Atlantic remained colder.

From June to November of 2008, cold water remained in the central Pacific, with warmer SSTs in the eastern Pacific, while water in the north and central Atlantic was also warmer and there were positive rainfall anomalies over the northwest Amazon basin.

From December 2008 to February 2009, the Pacific SSTs presented an inverse signal, with warm water throughout the whole Pacific basin, but positive rainfall anomalies still persisting over the northwest Amazon basin.

The rainfall patterns in northwest South America only changed in March to May 2009, when negative rainfall anomalies were present, as a lagged response to the warming in the Pacific. In this period, a meridional dipole was present in the Atlantic, with negative SST anomalies in the North Atlantic and positive anomalies in the South Atlantic. This anomalous southern shift of warmer SSTs in March–April 2009 corroborates the results of Foltz et al. (2012), such as the positive rainfall anomalies over northeast Brazil. Simultaneously, in the Pacific area, the SST anomalies configure the presence of a positive phase of an El Niño Modoki event, with warmer waters in the central Pacific and colder waters in the eastern Pacific. Despite the La Niña Modoki event that occurred during the whole of 2008, the southward shift of the ITCZ was also detected here, as reported by Foltz et al. (2012). Both events in the Pacific and Atlantic contributed to the increase of rainfall in the north of the Amazon basin throughout 2008 and at the beginning of 2009, which subsequently increased the river discharge anomalies.

To follow the sequence of events, the EMI signal was analyzed with 4 month-lagged rainfall and river discharge normalized anomalies. The rainfall anomalies were constructed with the spatially averaged rainfall in the area of 0°–12°N and 53°–70°W, over the 46 year period, but the analysis was restricted between March 2008 and September 2009, as shown in **Figure 10**. The negative phase of El Niño Modoki preceded the positive rainfall anomalies that peaked in March 2009, with a 2 month lag to the strong river discharge anomaly, while the maximum southward shift of the ITCZ occurred in March–May.

From March to May of 2008 (**Figure 9**), a clockwise vortex of surface winds was present over the northern part of South America and a second clockwise vortex was located over the eastern central Pacific, resulting in strong winds coming from the central Atlantic. In addition to this surface wind pattern, we analyzed the omega field (height × time), averaged over a section between 75° and 80°W and fixed at 5°N. The omega field represents the rate of change of pressure in a parcel over time (dp/dt), which is proportional to the vertical wind under hydrostatic balance. The vertical component of velocity in the pressure coordinates is positive in the downward direction. In this averaged section, we identified a strong ascending cell in the hovmöller diagram of the omega field (**Figure 11**). The upward vertical motion was represented by negative omega values, along the second half of 2008, from the surface to 200 hPa in the atmosphere. The ascending vertical motion favors the formation of convective clouds over the area. In this particular case, it seems to be that both phenomena contributed to an anomalous rainfall in the north of Amazon basin, consequently increasing a 2-month lagged Amazon River discharge anomaly in May of 2009.

Our EOF analysis revealed an influence of La Niña Modoki events in the spatial pattern of precipitation in the Amazon Basin, highlighting the positive anomalies in the northwest portion of the Amazon Basin. These rainfall patterns were associated with

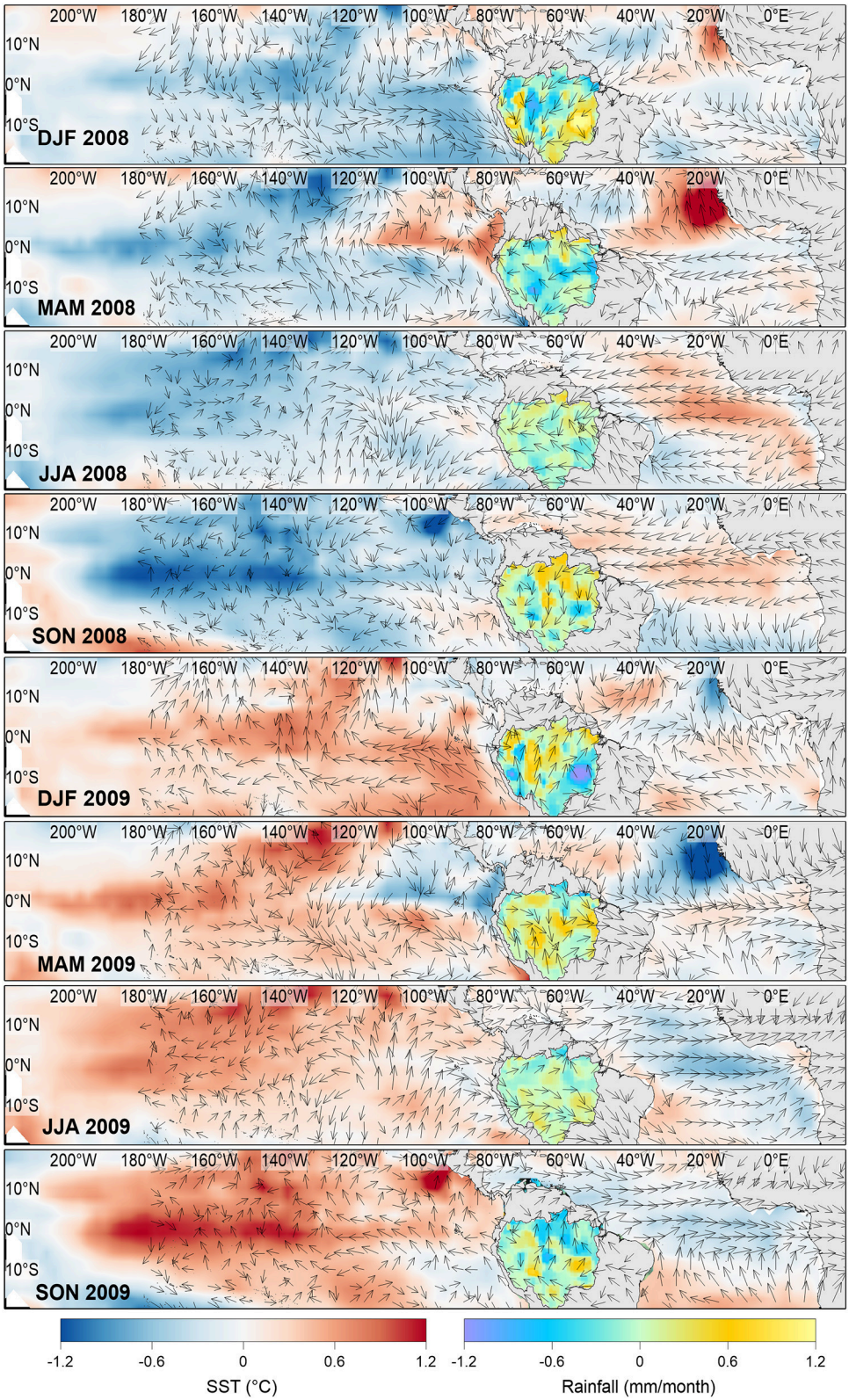

FIGURE 9 | Three-month composites of SST, rainfall (normalized scale by 10^3) and surface wind anomalies, from December 2007 to November 2009. Anomalies of SST and rainfall were constructed over the period of 46 years.

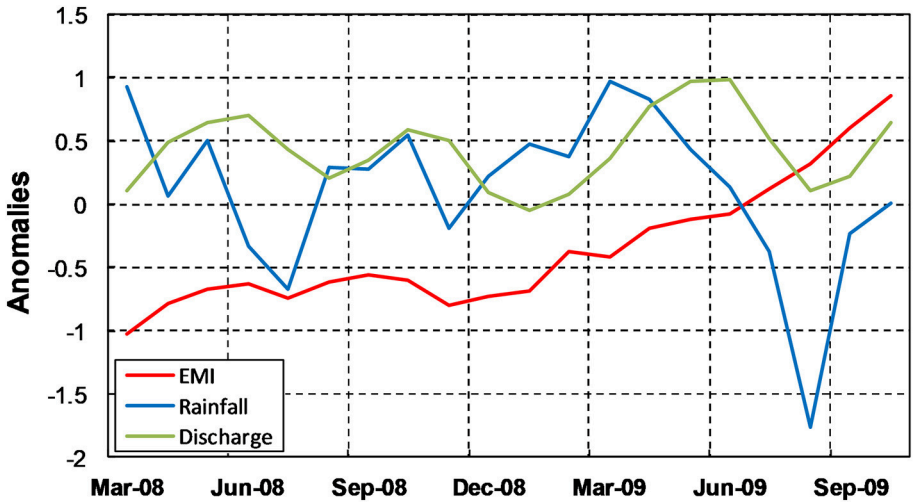

FIGURE 10 | Monthly normalized anomalies of rainfall (mm/month), computed over the area of 0°–12°N and 53°–70°W (blue line), Amazon River discharge (m^3 s^{-1}) (green line) and EMI (red line) shifted + 4 months. Anomalies of SST and rainfall were constructed over the period of 46 years.

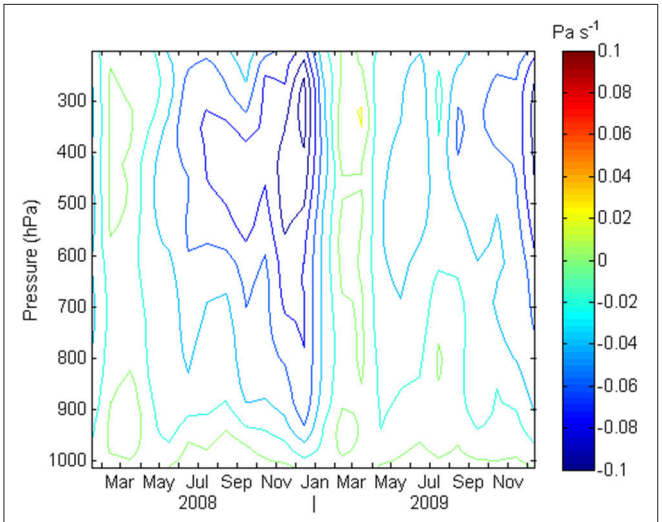

FIGURE 11 | Hovmöller diagram of monthly omega or vertical component of velocity in pressure coordinates (dp/dt), from 2008 to 2009, fixed at 5°N and averaged between 75°and 80°W. Omega is positive down (Pa s^{-1}).

the low SSS pattern in the Amazon River plume. In addition, our analysis focused on the specific period of 2008/2009, showing that La Niña Modoki events associated with an anomalous shift of the ITCZ in the Atlantic, had an important role in the development of convergence over the Amazon basin. Future studies should undertake an individual analysis of each Modoki event, which would improve these analyses and contribute to a better understanding of the role of La Niña Modoki events on the Amazon basin and river discharge. In addition, the influence of land rainfall vs ocean rainfall was quantified through a cross-correlation between the PC associated with EOF4 (rainfall vs. SSS), and the rainfall anomalies over the land and ocean.

We used the rainfall anomalies from the GPCP 2.3 dataset, once it covers both ocean and land precipitations. The results of the cross-correlation analysis between EOF4 PCs and rainfall anomalies are shown in **Figure 12**. The cross-correlation map indicated that, the PC (rainfall series) of EOF4 (rainfall vs. SSS) was associated with rainfall anomalies over the continent.

CONCLUSIONS

We used 46 years of ocean and atmospheric reanalysis data to show that interannual Pacific and Atlantic SST patterns can lead to different rainfall responses over the Amazon basin and, consequently can drive different interannual patterns in the SSS over the WTNA. The co-variability of SST and Amazon rainfall, and Amazon rainfall and surface salinity were examined using an EOF analysis. As in previous studies, links were found between El Niño and Atlantic indices and Amazon rainfall. The co-variability between rainfall and SSS demonstrated the existence of a strong positive SSS pattern along the coast. This was connected to negative rainfall anomalies over the whole of the Amazon basin, and was linked to canonical El Niño events. A second pattern also presented positive coastal SSS anomalies, when rainfall occurred predominantly over the northwestern part of the Amazon basin, with low rainfall around the Amazon River mouth.

The fourth EOF (rainfall vs. SSS) had the lowest salinity pattern in the WTNA. This pattern was associated with the third EOF (SST vs. rainfall), when positive rainfall anomalies were concentrated in the northwest part of the Amazon basin. This relationship was confirmed through a linear regression between the two analyses. The low SSS pattern linked to this mode was characterized by a spatial structure similar to the Amazon plume dispersion, with an eastward retroflection following the pathway of the NECC. From the EOF and correlation analysis, we identified the negative phase of El Niño Modoki events as

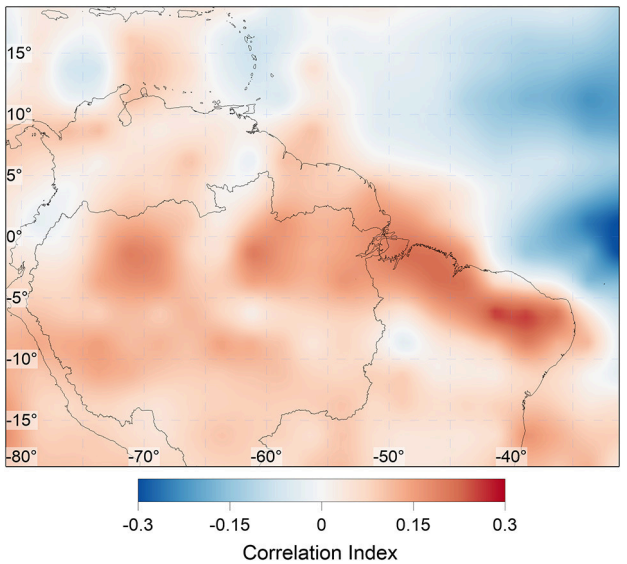

FIGURE 12 | Cross-correlation between EOF4 principal component and GPCP rainfall anomalies over land and ocean, from 1979 to 2015.

the main contributor to this mode. However, a detailed analysis was conducted for the years of 2008 and 2009, when anomalous rainfall in the north of the Amazon basin occurred, followed by an intense Amazon River discharge. During 2008 a La Niña Modoki event occurred and in April–May of 2009 an anomalous southward shift of the ITCZ took place. Both phenomena resulted in increased SST anomalies in the southwest Atlantic and eastern Pacific, contributing to an intensification of the convergence of ocean winds to the continent. The convergence of surface winds contributed to a strong vertical cell of ascending winds that was present over the north of the Amazon basin from the surface to 200 hPa. In this particular case, both phenomena contributed to anomalous rainfall in the north of the Amazon basin, consequently increasing a 2-month lagged Amazon River discharge anomaly in May of 2009.

Despite this particular case, the statistical analysis of the 46 year period indicated that La Niña Modoki events were important contributors to low SSS in the Amazon River plume. Our correlation results also provided evidence that the rainfall mode, associated with La Niña Modoki, responded better to rainfall anomalies over the continent. However, it is important to consider that not all SSS variability in the WTNA could be explained by changes in the Amazon discharge. Oceanic rainfall as well as advection are also important forcings of the SSS variability in this region, with strong boundary currents and strong SSS gradients created by the Amazon outflow, even in the absence of discharge anomalies. This pattern of low salinity makes an important contribution to other processes, such as an increase in productivity, and changes in the surface dynamics, mixed layer thickness, CO_2 fluxes, and light absorption. For example, light absorption is significantly enhanced in low salinity regimes (Subramanian et al., 2008), suggesting that the ocean color in the plume area can be traced back to the freshwater discharge. In addition, the SSS in the Amazon plume has consequences for air-sea CO_2 exchange and has an impact on biogeochemical cycles. In the WTNA, surface waters with low salinity (<35) are usually a sink of CO_2 from the atmosphere. The magnitude of these processes can be intensified according to the magnitude and frequency of El Niño Modoki events.

AUTHOR CONTRIBUTIONS

PT and DV conceived the idea. PT, DV, NL, MA, JS, GC, CN, and TS performed the data acquisition and analysis, and all authors contributed extensively to the interpretation and analysis of the results, and the production of the final manuscript.

FUNDING

PT acknowledges the PhD scholarship support of the Higher Education Personnel Training Coordination (Coordination for the Improvement of Higher Education Personnel (CAPES)—Brazil). CN acknowledges the Coordination for the Improvement of Higher Education Personnel–CAPES (DICAM project, grant 1975/2014). This paper contributes to the Brazilian Research Network on Global Climate Change, FINEP/Rede CLIMA Grant Number 01.13.0353-00. The authors thank the Project ProdPluma—*Modelo Regional de Produtividade Primária da Pluma do Amazonas* (CNPq grant 460687/2014-0), European Integrated CARBOCHANGE (FP7 264879), and the Brazilian National Institute of Science and Technology for Tropical Marine Environments–INCT AmbTropic (CNPq/FABESB grants 565054/2010-4 and 8936/2011). JS thanks CNPq for supporting the Project *Mudanças Climáticas no Atlântico Tropical—MUSCAT*, (CNPq grant 400544/2013-0) and *Fundação Cearense de Meteorologia e Recursos Hídricos—FUNCEME (Edital 01/2016)* for its support during the placement of JS at Fortaleza, CE, Brazil. This paper is also part of the Project *Pólo de Interação para o Desenvolvimento de Estudos conjuntos em Oceanografia do Atlântico Tropical–PILOTE* (CNPq-IRD grant 490289/2013-4).

ACKNOWLEDGMENTS

The authors would like to thank the National Oceanic and Atmospheric Administration's (NOAA) Oceanic and Atmospheric Research (OAR) Earth System Research Laboratory (ESRL) Physical Sciences Division (PSD), Boulder, Colorado, USA, for providing GPCC Precipitation data from their Web site at http://www.esrl.noaa.gov/psd/. We appreciate the provision of Weather Forecast-Ocean Reanalysis-4 (ECMWF-ORAS4) data by the Integrated Climate Data Center at the University of Hamburg. The authors would like to thank the SO-HYBAM observatory for providing discharge data [www.ore-hybam.org]. The ERA-Interim data were made available courtesy of ECMWF. We would like to thank both reviewers for their valuable suggestions and comments on the paper.

REFERENCES

Araujo, M., Noriega, C., and Lefèvre, N. (2014). Nutrients and carbon fluxes in the estuaries of major rivers flowing into the tropical Atlantic. *Front. Mar. Sci.* 1:10. doi: 10.3389/fmars.2014.00010

Ashok, K., and Yamagata, T. (2009). Climate change: the El Niño with a difference. *Nature* 461, 481–484. doi: 10.1038/461481a

Ashok, K., Behera, S. K., Rao, S. A., Weng, H., and Yamagata, T. (2007). El Niño Modoki and its possible teleconnection. *J. Geophys. Res. Oceans* 112, 1–27. doi: 10.1029/2006JC003798

Balaguru, K. Chang, P., Saravanan, R. Leung, L. R., Xu, Z., Li, M., et al. (2012). Ocean Barrier layers' effect on tropical cyclone intensification. *Proc. Natl. Acad. Sci. U.S.A.* 109, 14343–14347. doi: 10.1073/pnas.1201364109

Balmaseda, M. A., Mogensen, K., and Weaver, A. T. (2013). Evaluation of the ECMWF ocean reanalysis system ORAS4. *Q. J. R. Meteorol. Soc.* 139, 1132–1161. doi: 10.1002/qj.2063

Beluco, A., and Souza, P. K. D. (2014). Energy at the junction of the rivers Negro and Solimões, contributors of the Amazon River, in the Brazilian Amazon. *Int. Schol. Res. Notic.* 2014:79458. doi: 10.1155/2014/794583

Bretherton, C., Smith, C., and Wallace, J. (1992). An Intercomparison of methods for finding coupled patterns in climate data. *J. Clim.* 5, 541–560. doi: 10.1175/1520-0442(1992)005%3C0541: AIOMFF%3E2.0.CO;2

Coles, V. J., Brooks, M. T., Hopkins, J., Stukel, M. R., Yager, P. L., and Hood, R. R. (2013). The pathways and properties of the Amazon River Plume in the tropical North Atlantic Ocean. *J. Geophys. Res. Oceans* 118, 6894–6913. doi: 10.1002/2013JC008981.

Di Lorenzo, E., Liguori, G., Schneider, N., Furtado, J. C., Anderson, B. T., and Alexander, M. A. (2015). ENSO and meridional modes: a null hypothesis for Pacific climate variability. *Geophys. Res. Lett.* 42, 9440–9448. doi: 10.1002/2015GL066281

Du, Y., Zhang, Y., Feng, M., Wang, T., Zhang, N., and Wijffels, S. (2015). Decadal trends of the upper ocean salinity in the tropical Indo-Pacific since mid-1990s. *Sci.Rep.* 5:16050. doi: 10.1038/srep16050

Ferry, N., and Reverdin, G. (2004). Sea surface salinity interannual variability in the western tropical Atlantic: an ocean general circulation model study. *J. Geophys. Res.* 109, C05026. doi: 10.1029/2003JC002122

Foltz, G. R., Schmid, C., and Lumpkin, R. (2015). Transport of surface freshwater from the equatorial to the subtropical North Atlantic Ocean. *J. Phys. Oceanogr.* 45, 1086–1102. doi: 10.1175/JPO-D-14-0189.1

Foltz, G. R., McPhaden, M. J., and Lumpkin, R. (2012). A strong atlantic meridional mode event in 2009: the role of mixed layer dynamics. *J. Clim.* 25, 363–380. doi: 10.1175/JCLI-D-11-00150.1

Geider, J. R., DeLucia, H. E., Falkowski, G. P., Finzi, C. A., Philip Grime, J., Grace, J., et al. (2001). Primary productivity of planet earth: biological determinants and physical constraints in terrestrial and aquatic habitats. *Glob. Chan. Biol.* 7, 849–882. doi: 10.1046/j.1365-2486.2001.00448.x

Grimm, A. M. (2003). The El Niño impact on summer monsoon in Brazil: regional processes versus remote influences. *J. Clim.* 16, 263–280. doi: 10.1175/1520-0442(2003)016<0263:TENIOT>2.0.CO;2

Grimm, A. M. (2004). How do La Niña events disturb the summer monsoon system in Brazil? *Clim. Dyn.* 22, 123–138. doi: 10.1007/s00382-003-0368-7

Grimm, A. M., Barros, V. R., and Doyle, M. E. (2000). Climate variability in southern South America associated with El Niño and La Niña events. *J. Clim.* 13, 35–58. doi: 10.1175/1520-0442(2000)013<0035:CVISSA>2.0.CO;2

Grodsky, S. A., Carton, J. A., and, Bryan, F. O. (2014a). A curious local surface salinity maximum in the northwestern tropical Atlantic. *J. Geophys. Res. Oceans* 119, 484–495. doi: 10.1002/2013JC009450

Grodsky, S. A., Johnson, B. K., Carton, J. A., and Bryan, F. O. (2015). Interannual Caribbean salinity in satellite data and model simulations. *J. Geophys. Res. Oceans* 120, 1375–1387. doi: 10.1002/2014JC010625

Grodsky, S. A., Reul, N., Lagerloef, G., Reverdin, G., Carton, J. A., Chapron, B., et al. (2012). Haline hurricane wake in the Amazon/Orinoco plume: AQUARIUS/SACD and SMOS observations. *Geophys. Res. Lett.* 39, L20603. doi: 10.1029/2012GL053335

Grodsky, S. A., Reverdin, G., Carton, J. A., and Coles, V. J. (2014b). Year-to-year salinity changes in the Amazon plume: contrasting 2011 and 2012 Aquarius/SACD and SMOS satellite data. *Remote Sens. Environ.* 140, 14–22. doi: 10.1016/j.rse.2013.08.033

Hellweger, F. L., and Gordon, A. L. (2002). Tracing Amazon River water into the Caribbean Sea. *J. Mar. Res.* 60, 537–549. doi: 10.1357/002224002762324202

Ibánhez, J. S. P., Flores, M., and Lefèvre, N. (2017). Collapse of the tropical and subtropical North Atlantic CO_2 sink in boreal spring of 2010. *Sci.Rep.* 7:41694. doi: 10.1038/srep41694

Jiménez-Muñoz, J. C., Mattar, C., Barichivich, J., Santamaría-Artigas, A., Takahashi, K., Malhi, Y., et al. (2016). Record-breaking warming and extreme drought in the Amazon rainforest during the course of El Niño 2015–2016. *Sci. Rep.* 6:33130. doi: 10.1038/srep33130

Johns, W. E., Lee, T. N., Beardsley, R. C., Candela, J., Limeburner, R., and Castro, B. (1998). Annual cycle and variability of the North Brazil Current. *J. Phys. Oceanogr.* 28, 103–128.

Kao, H.-Y., and, Yu, J.-Y. (2009). Contrasting Eastern-Pacific and Central-Pacific Types of ENSO. *J. Clim.* 22, 615–632. doi: 10.1175/2008JCLI2309.1

Kelly, P. S., Lwiza, K. M. M., Cowen, R. K., and Goni, G. J. (2000). Low-salinity pools at Barbados, West Indies: their origin, frequency, and variability. *J. Geophys. Res.* 105, 19699–19708. doi: 10.1029/1999JC900328

Korosov, A., Counillon, F., and, Johannessen, J. A. (2015). Monitoring the spreading of the Amazon freshwater plume by MODIS, SMOS, Aquarius, and TOPAZ. *J. Geophys. Res. Oceans* 120, 268–283. doi: 10.1002/2014JC010155

Körtzinger, A. (2003). A significant CO_2 sink in the tropical Atlantic Ocean associated with the Amazon River plume. *Geophys. Res. Lett.* 30, 2287. doi: 10.1029/2003GL01884124

Kulkarni, M. N., and Siingh, D. (2016). The atmospheric electrical index for ENSO modoki: is ENSO Modoki one of the factors responsible for the warming trend slowdown? *Sci. Rep.* 6:24009. doi: 10.1038/srep24009

Lefèvre, N., Diverrès, D., and Gallois, F. (2010). Origin of CO_2 undersaturation in the western tropical Atlantic. *Tellus Ser. B Chem. Phys. Meteorol.* 62, 595–607. doi: 10.1111/j.1600-0889. 2010.00475.x

Lentz, S. J. (1995). Seasonal variations in the horizontal structure of the Amazon Plume inferred from historical hydrographic data. *J. Geophys. Res.* 100, 2391–2400. doi: 10.1029/94JC01847

Li, W., Zhang, P., Ye, J., Li, L., and Baker, P. A. (2011). Impact of two different types of El Niño events on the amazon climate and ecosystem productivity. *J. Plant Ecol.* 4, 91–99. doi: 10.1093/jpe/rtq039

Marengo, J. A. (1992). Interannual variability of surface climate in the Amazon basin. *Int. J. Clim.* 12, 853–863. doi: 10.1002/joc.3370120808

Marengo, J. A., Alves, L. M., Soares, W. R., Rodriguez, D. A., Camargo, H., Riveros, M., et al. (2013). Two Contrasting Severe Seasonal Extremes in Tropical South America in 2012: flood in Amazonia and Drought in Northeast Brazil. *J. Clim.* 26, 9137–9154. doi: 10.1175/JCLI-D-12-00642.1

Marengo, J. A., and Espinoza, J. C. (2015). Extreme seasonal droughts and floods in Amazonia: causes, trends and impacts. *Int. J. Clim.* 36, 1033–1050. doi: 10.1002/joc.4420

Marengo, J. A., Nobre, C. A., Tomasella, J., Oyama, M. D., Sampaio de Oliveira, G., de Oliveira, R., et al. (2008). The drought of Amazonia in 2005. *J. Clim.* 21, 495–516. doi: 10.1175/2007JCLI1600.1

McPhaden, M. J., Lee, T., and McClurg, D. (2011). El Niño and its relationship to changing background conditions in the tropical Pacific Ocean. *Geophys. Res. Lett.* 38:L15709. doi: 10.1029/2011GL048275

Misra, V. (2008a). Coupled interactions of the monsoons. *Geophys. Res. Lett.* 35, L12705. doi: 10.1029/2008GL033562

Misra, V. (2008b). Coupled air, sea, and land interactions of the South American monsoon. *J. Clim.* 21, 6389–6403. doi: 10.1175/2008JCLI2497.1

Muller-Krager, F. E., McClain, C. R., and Richardson, P. L. (1988). The dispersal of the Amazon water. *Nature* 333, 56–59.

Paegle, J. N., and Mo, K. C. (2002). Linkages between summer rainfall variability over South America and sea surface temperature anomalies. *J. Clim.* 15, 1389–1407. doi: 10.1175/1520-0442(2002)015<1389:LBSRVO>2.0.CO;2

Ronchail, J., Cochonneau, G., Molinier, M., Guyot, J. L., Chaves, A. G. D., Guimarães, V., et al. (2002). Interannual rainfall variability in the Amazon basin and sea-surface temperatures in the equatorial Pacific and the tropical Atlantic Oceans. *Int. J. Clim.* 22, 1663–1686. doi: 10.1002/joc.815

Salisbury, J., Vandemark, D., Campbell, J., Hunt, C., Wisser, D., Reul, N., et al. (2011). Spatial and temporal coherence between Amazon River discharge, salinity, and light absorption by colored organic carbon in western tropical Atlantic surface waters. *J. Geophys. Res.* 116:C00H02. doi: 10.1029/2011JC006989

Schmitt, R. N. W. (2008). Salinity and the global water cycle. *Oceanography* 21, 12–19. doi: 10.5670/oceanog.2008.63

Schneider, U., Becker, A., Finger, P., Meyer-Christoffer, A., Rudolf, B., and Ziese, M. (2015). GPCC full data reanalysis version 7.0 at 0.5°: monthly land-surface precipitation from rain-gauges built on GTS-based and historic Data. doi: 10.5676/DWD_GPCC/FD_M_V7_050

Schneider, U., Becker, A., Finger, P., Meyer-Christoffer, A., Ziese, M., and Rudolf, B. (2014). GPCCS's new land surface precipitation climatology based on quality-controlled *in situ* data and its role in quantifying the global water cycle. *Theor. Appl. Climatol.* 115, 15–40. doi: 10.1007/ s00704-013-0860-x

Shinoda, T., Hurlburt, H. E., and Metzger, E. J. (2011). Anomalous tropical ocean circulation associated with La Niña Modoki. *J. Geophys. Res.* 116, C12001. doi: 10.1029/2011JC00730

Smith, W. O. Jr., and Demaster, D. J. (1996). Phytoplankton and biomass productivity in the Amazon river plume: correlation with seasonal river discharge. *Cont. Shelf Res.* 16, 291–317.

Subramanian, A., Yager, P. L., Carpenter, E. J., Mahaffey, C., Bjorkman, K., Cooley, S., et al. (2008). Amazon River enhances diazotrophy and carbon sequestration in the tropical north Atlantic Ocean. *Proc. Natl. Acad. Sci. U.S.A.* 105, 10460–10465. doi: 10.1073/pnas.0710279105

Uvo, C., Repelli, C. A., Zebiak, S. E and Kushnir, Y. (1998). The relationships between tropical Pacific and Atlantic SST and Northeast Brazil monthly precipitation. *J. Clim.*, 11, 551–562. doi: 10.1175/1520-0442(1998)011<0551:TRBTPA>2.0.CO;2

Wallace, J., Smith, C., and Bretherton, C. (1992). Singular value decomposition of wintertime sea surface temperature and 500-mb height anomalies. *J. Clim.* 5, 561–576. doi: 10.1175/1520-0442(1992)005%3C0561:SVDOWS%3E2.0.CO;2

Weng, H., Ashok, K., Behera, S. K., Rao, S. A., and Yamagata, T. (2007). Impacts of recent El Niño Modoki on dry/wet conditions in the pacific rim during boreal summer. *Clim. Dyn.* 29, 113–129. doi: 10.1007/s00382-007-0234-0

Wisser, D., Fekete, B. M., Vörösmarty, C. J., and Schumann, A. H. (2010). Reconstructing 20th century global hydrography: a contribution to the Global Terrestrial Network- Hydrology (GTN-H). *Hydrol. Earth Syst. Sci.* 14, 1–24. doi: 10.5194/hess-14-1-2010

Xie, F., Li, J., Tian, W., Li, Y., and Feng, J. (2014). Indo-pacific warm pool area expansion, Modoki activity, and tropical cold-point tropopause temperature variations. *Sci. Rep.* 4:4552. doi: 10.1038/srep04552

Yeh, S. W., Kug, J. S., Dewitte, B., Kwon, M.-H., Kirtman, B. P., and Jin, F. F. (2009). El Niño in a changing climate. *Nature* 461, 511–514. doi: 10.1038/nature08316

Yeh, S.-W., and B. P., Kirtman (2004). Tropical Pacific decadal variability and ENSO amplitude modulations in a CGCM. *J. Geophys. Res.* 109, C11009. doi: 10.1029/2004JC002442

Yu, J. Y., Kao, H. Y., and Lee, T. (2010). Subtropics-related interannual sea surface temperature variability in the central equatorial pacific. *J. Clim.* 23, 2869–2884. doi: 10.1175/2010JCLI3171.1

Yu, L., Jin, X., and Weller, R. A. (2007). Annual, seasonal, and interannual variability of air-sea heat fluxes in the Indian Ocean. *J. Clim.* 20, 3190–3209. doi: 10.1175/JCLI4163.1

Conflict of Interest Statement: The authors declare that the research was conducted in the absence of any commercial or financial relationships that could be construed as a potential conflict of interest.

Copyright © 2017 Tyaquiçã, Veleda, Lefèvre, Araujo, Noriega, Caniaux, Servain and Silva. This is an open-access article distributed under the terms of the Creative Commons Attribution License (CC BY). The use, distribution or reproduction in other forums is permitted, provided the original author(s) or licensor are credited and that the original publication in this journal is cited, in accordance with accepted academic practice. No use, distribution or reproduction is permitted which does not comply with these terms.